

Cosmic Axions Revealed via Amplified Modulation of Ellipticity of Laser (CARMEL)

Hooman Davoudiasl¹ and Yannis K. Semertzidis^{2,*}

¹*High Energy Theory Group, Physics Department,
Brookhaven National Laboratory, Upton, New York 11973, USA*

²*Department of Physics, Korea Advanced Institute of Science and Technology (KAIST), Daejeon 34141, Republic of Korea*

We propose a new axion dark matter detection strategy that employs optical readout of laser beam ellipticity modulations caused by axion-induced electric fields in a microwave cavity, using electro-optic (EO) crystals, enhanced by externally injected radio-frequency (RF) power. Building upon the variance-based probing method [1], we extend this concept to the optical domain: a weak probe laser interacts with an EO crystal placed inside a resonant microwave cavity at cryogenic temperatures, and the axion-induced electric field is revealed through induced ellipticity. The injected RF signal coherently interferes with that of the axion field, amplifying the optical response and significantly improving sensitivity. While our EO-based method employs a Fabry-Pérot resonator, we do not require Michelson interferometers. Our method hence enables compact, high-frequency axion searches, across the 0.5-50 GHz range. Operating at cryogenic temperatures not only suppresses thermal backgrounds but, critically, allows the probing method to mitigate the laser quantum noise. This approach offers a scalable path forward for axion detection over the \sim (few – 200) μeV mass range – covering the preferred parameter space for the post-inflationary Peccei-Quinn axion dark matter – using compact, tunable systems.

I. INTRODUCTION

The identity of dark matter (DM) remains one of the most compelling unsolved problems in fundamental physics. Among the theoretically favored candidates is the quantum chromodynamics (QCD) axion a [2, 3], associated with the Peccei-Quinn (PQ) mechanism [4, 5] originally introduced to resolve the strong CP problem, *i.e.* the puzzling smallness of the CP violating parameter in QCD. The axion of the PQ framework emerges as a natural cold dark matter candidate, with its abundance determined by early-universe dynamics [6–8]. For a recent article on the resilience of the strong CP problem, see Ref. [9].

The mass m_a of the QCD axion DM is expected to have a narrow viable range if the associated PQ symmetry is broken after inflation in the early Universe (see, for example, Ref. [10]). Cosmological and lattice calculations suggest that post-inflationary scenarios prefer an axion mass in the tens to hundreds of μeV [11–16] range, with a recent analysis suggesting $40 \mu\text{eV} < m_a < 180 \mu\text{eV}$ [17]. This mass range can be well covered by resonant cavity technique proposed below, in the photon frequency range 0.5-50 GHz, which will be the focus of our discussion.

The most sensitive experimental approach to detecting axions in the above mass window is the haloscope technique, which exploits axion-photon conversion in a resonant microwave cavity permeated by a strong magnetic field, as was suggested first by Sikivie [7]. However, haloscopes face a fundamental limitation: as the resonant frequency increases, the physical volume of the cavity—and hence the signal power—must decrease. For an ax-

ion signal at 25 GHz, a natural cavity volume is $\sim 1 \text{ cm}^3$, over $10^5 \times$ smaller than the volumes used in the original ADMX configuration [18–22]. Covering the 0.5-50 GHz range at half the resolution matched to the axion coherence bandwidth, $\Delta\nu/\nu \sim 10^{-6}$, requires $\sim 10^7$ distinct frequency channels (the band width for axions is set by their small kinetic energy $\propto v^2$, where $v \sim 10^{-3}$ is the virial velocity in our galactic neighborhood). This scaling imposes a stringent limitation on scanning speed, primarily because conventional readout electronics contribute significant quantum or thermal noise, requiring long integration times per frequency channel. For example, assuming a typical $\sim 100 \text{ s}$ integration time per bin, covering the above frequency range would take ~ 30 years. By contrast, our proposed axion signal probing method, based on laser readout through a Fabry-Pérot interferometer and electro-optic modulation, effectively bypasses the limitations of traditional RF electronics. It enables sensitivity well beyond the quantum noise floor typically imposed by the detection system. The method proposed here can potentially speed up scanning rates by more than an order of magnitude, using available technology.

Current state-of-the-art experiments in this regime rely on ultra-low-noise amplifiers, quantum-limited detectors, and often large optical interferometers or complex cavity geometries. Yet, sensitivity improvements remain incremental, and the ability to scan efficiently across millions of channels with sufficient signal-to-noise ratio (SNR) remains out of reach. A fundamentally different approach is required to break through this bottleneck—one that enables enhanced sensitivity even in small volumes, with suppressed noise, and minimal reliance on ultra-complex cryogenic amplification chains.

The current status of axion searches is summarized by the plot in Fig.1, taken from Ref. [23]. As can be seen here, the window corresponding to the preferred post-

* Corresponding author; yannis@kaist.ac.kr

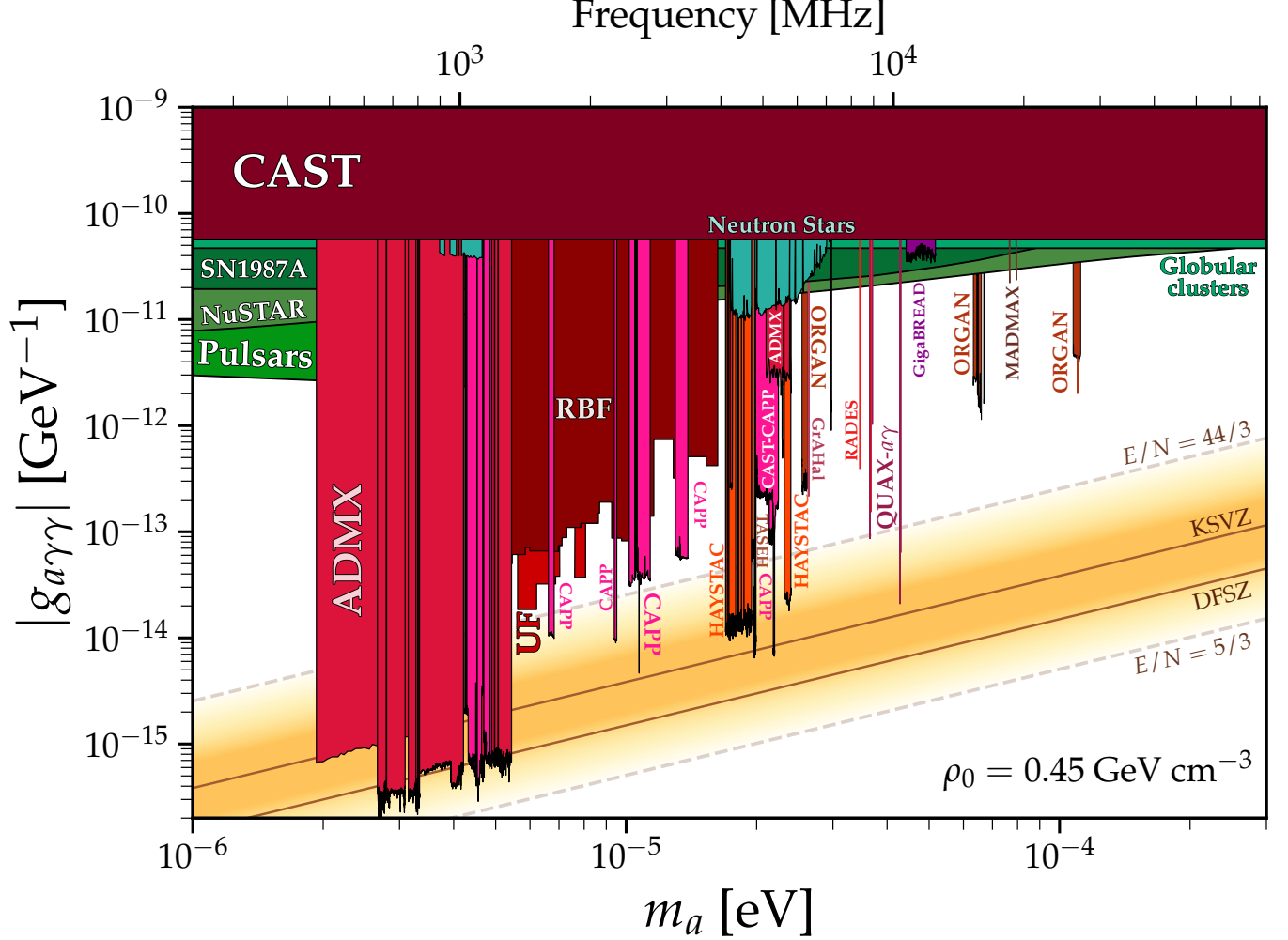


FIG. 1: The current status of the axion to two photon coupling in the mass range 1-300 μeV , corresponding to the frequency range 0.2-70 GHz (from Ref. [23]). CAMEL aims to facilitate probing the frequency range of 0.5-50 GHz, or $\sim (2-200)$ μeV , with better than DFSZ sensitivity within the next five years. CAMEL can potentially cover the preferred post-inflationary parameter space, corresponding to 40-180 μeV [17], at better than DFSZ sensitivity, using presently available technical capabilities.

inflationary PQ axion DM, $\sim 40 - 180$ μeV , within the KSVZ [24, 25] and DFSZ [8, 26] scenarios, remains largely unexplored. This hints at the inherent challenges associated with this regime of parameters. Progress in this range has been slow due to the convergence of several technical challenges: the cavity volume decreases with increasing frequency, conventional copper cavities suffer from degraded quality factors at high frequencies, and quantum-limited linear amplifiers constrain the readout sensitivity. Meanwhile, single-photon detectors, though promising, are not yet mature for robust operation under realistic laboratory conditions.

To overcome these barriers, multiple high-frequency haloscope concepts are under active development. These include the pizza-cavity design [27], which partitions the

cavity into multiple sectors to increase frequency while preserving volume efficiency; photonic crystal [28, 29] and metamaterial cavities [30], which decouple frequency from physical size; and horn-array haloscopes [31], which leverage large metal surface areas to achieve broadband, volume-efficient searches at high frequencies. Additionally, pioneering experiments such as MADMAX [32–34], and DALI [35] explore dielectric haloscope techniques using layered dielectric interfaces to coherently boost the axion-induced signal power. ALPHA using the electron plasma resonance frequency of metallic rods [36], and CAST-CAPP [37] using a decommissioned dipole magnet in an efficient geometry. Superconducting cavities with quality factors comparable to or exceeding the expected axion quality factor, even in the presence of strong

magnetic fields (~ 8 T and above), have been demonstrated using high-temperature superconducting (HTS) tapes [38–40]. These developments indicate that this technology is maturing and offer a scalable path toward detecting axions in the tens to hundreds of μeV mass range, as motivated by post-inflation QCD axion models.

In parallel, we introduce CARMEL (Cosmic Axions Revealed via Amplified Modulation of Ellipticity of Laser), a novel detection technique that mitigates the effects of quantum noise and replaces conventional amplifier chains with optical readout. CARMEL detects the axion-induced microwave field via its modulation of a laser beam polarization or phase, thus bypassing the quantum noise limitations of linear amplification. Importantly, this method is not limited to high frequencies: it can also be applied at lower frequencies (e.g., near 200 MHz), where electronic noise in standard amplifiers is still far above the quantum limit. In these cases, CARMEL can yield sensitivity improvements of up to several orders of magnitude, making it a transformative technique for axion detection across the full spectrum from sub-GHz to tens of GHz.

Our proposal combines electro-optic (EO) detection [41] and a “resonant probing” technique [1], see also [42–44]. These methods, previously suggested independently, are now unified to offer:

1. Sensitivity mitigating the quantum noise limit at low temperatures, and
2. Operation with only modest laser power (1–10 mW).

This approach is also applicable to other experimental geometries, including MADMAX and related dielectric haloscope designs [32–36].

Next, we will discuss the basics of the axion detection in our proposed setup. We will provide estimates for the signal and main sources of noise. Our analysis will illustrate that the SNR achieved can lead to a definitive detection across and beyond the post-inflationary

PQ axion DM parameter space, employing technology that is currently available. Henceforth, we shall assume a laser with power $P = 10 \text{ mW} = 10^{-2} \text{ W}$ and wavelength $\lambda = 1064 \text{ nm} \Rightarrow \nu = c/\lambda \approx 2.82 \times 10^{14} \text{ Hz}$, where ν is the laser beam frequency; $h = 6.626 \times 10^{-34} \text{ J s}$ is Planck’s constant.

II. DETECTION PRINCIPLE

The basis of our proposal is the use of the EO effect, where an electric field $E \equiv |\vec{E}|$ leads to induced ellipticity ψ in a laser beam of wavelength λ (Pockels effect [45, 46]). We have

$$\psi = \frac{\pi}{\lambda} n^3 r_{ij} E L, \quad (1)$$

where n is refractive index of the EO crystal, r_{ij} is assumed to be the largest element of the EO coefficient tensor, and L is the length of the crystal through which the laser propagates.

Let us now estimate the contribution of axion conversion in a cavity to the above effect. The power output from axion-to-photon conversion in a microwave cavity operating in the TM_{010} mode, using experimental parameters as reported by CAPP, is given by [47, 48]:

Parameter	Value
Laser Power	10 mW
Laser Wavelength	1064 nm
RF Probe Power	2 nW
Microwave Cavity Quality Factor Q_c	10^4
Axion-to-Photon Reference Power P_a ($Q_c = 10^4$)	10^{-23} W
Microwave Cavity Volume	3.7 L
Fabry-Pérot Finesse \mathcal{F}	10^4
EO Crystal (LiNbO_3) Thickness L	3 mm

TABLE I: Benchmark parameters assumed in this work, for the $\nu_a \sim O(10 \text{ GHz})$ regime.

$$P_{a\gamma\gamma} = 8.7 \times 10^{-23} \text{ W} \left(\frac{g_\gamma}{0.36} \right)^2 \left(\frac{\rho_a}{0.45 \text{ GeV/cm}^3} \right) \left(\frac{\nu_a}{1.1 \text{ GHz}} \right) \left(\frac{\langle \mathbf{B}_e^2 \rangle}{(10.3 \text{ T})^2} \right) \left(\frac{V}{37 \text{ L}} \right) \left(\frac{G}{0.6} \right) \left(\frac{10^6}{Q_a} + \frac{10^5}{Q_c} \right)^{-1}, \quad (2)$$

where $g_{a\gamma\gamma} = (\alpha/\pi)(g_\gamma/f_a)$ is the axion-photon coupling, α is the fine structure constant, and g_γ takes values of -0.97 (KSVZ model [24, 25]) or 0.36 (DFSZ model [8, 26]). ρ_a is the local axion dark matter density, and $\nu_a = m_a c^2/h$ is the axion Compton frequency ($c = 2.998 \times 10^8 \text{ m/s}$ is the speed of light). In the above, $\langle \mathbf{B}_e^2 \rangle$ is the squared average external magnetic field, V is the cavity volume, $Q_a \approx 10^6$ is the axion quality factor, and Q_c is the cavity unloaded quality factor. The form factor G

reflects the mode-dependent overlap of the axion-induced field with the resonant mode and is approximately 0.69 for the TM_{010} mode.

In the limit $Q_c \ll Q_a$, the signal power scales linearly with Q_c :

$$P_a \propto Q_c. \quad (3)$$

Conversely, for $Q_c \gg Q_a$, the signal power saturates:

$$P_a \approx (\text{constant}) \propto Q_a, \quad (4)$$

reflecting the finite spectral width of the axion signal; the cavity cannot enhance the signal beyond the axion's intrinsic coherence bandwidth.

The total power deposited by axion conversion is given by

$$P_a = \frac{\omega U}{Q_c}, \quad (5)$$

where P_a is the axion-induced power in Eq. (2), $\omega = 2\pi f$ is the angular frequency of the cavity (or the axion, on resonance), and U is the total stored energy in the cavity. Since the stored energy is equally partitioned between electric and magnetic components, the electric field energy is [49]

$$U_E = \frac{1}{2}\epsilon_0 V E_a^2 = \frac{U}{2} = \frac{P_a Q_c}{2\omega}, \quad (6)$$

where E_a is the root-mean-square electric field, $\epsilon_0 = 8.85 \times 10^{-12}$ F/m is the vacuum permittivity, and V is the cavity volume. Solving for E_a we get

$$E_a = \sqrt{\frac{P_a Q_c}{\omega \epsilon_0 V}}, \quad (7)$$

We will use $V = 3.7 \times 10^{-3} \text{ m}^3$ (3.7 liters) as a benchmark value in what follows, appropriate for a modified 10 GHz cavity. However, this volume is not a fixed requirement. At a given frequency, the cavity geometry may be adapted to vary V while maintaining resonance to satisfy a desired reference power level. This flexibility in cavity volume is particularly useful for optimizing sensitivity while staying within the physical constraints imposed by the detection scheme and available magnet apertures.

We will consider using lithium niobate, LiNbO_3 , of size $L = 3 \text{ mm}$, as our EO crystal, for which $n \approx 2.2$ and $r_{33} \approx 3.1 \times 10^{-11} \text{ m/V}$. Let us take $f = 10 \text{ GHz}$ as a representative value. We will consider the benchmark values $P_a = 10^{-23} \text{ W}$ and $Q_c = 10^4$ for the chosen value of f above. From Eqs.(1) and (7), we get $E_a \approx 7.0 \times 10^{-9} \text{ V/m}$ and $\psi_a \approx 2 \times 10^{-14} \text{ rad}$.

To determine the minimum detectable ellipticity, we need to estimate contributions from various sources of noise. We identify two main sources: (i) shot noise from the finite power output of the laser beam, and (ii) the quantum-thermal noise in the cavity. Here, we first examine the effect of shot noise and in the next sub-section we will discuss quantum-thermal effects.

(i) *Shot noise*: To estimate the photon shot noise, we use the standard expression

$$\delta\psi_{\text{shot-laser}} = \frac{\sqrt{2}}{\sqrt{P/h\nu}} = \sqrt{\frac{2h\nu}{P}} \quad (8)$$

where P is the laser power and ν is the associated frequency. Substituting our benchmark values we have

$$\delta\psi_{\text{shot-laser}} \approx 6.1 \times 10^{-9} \text{ rad} \cdot \text{Hz}^{-1/2} \quad (9)$$

For an integration time of $t = 3 \text{ seconds}$, assumed henceforth, we get

$$\delta\psi_{\text{shot-laser}} = \frac{6.1 \times 10^{-9}}{\sqrt{3}} \approx 3.5 \times 10^{-9} \text{ rad}. \quad (10)$$

Assuming only laser beam shot noise, we see that the expected typical SNR would be

$$\text{SNR}_{\text{laser}} = \frac{\psi_a}{\delta\psi_{\text{shot}}} \approx 6 \times 10^{-6}, \quad (11)$$

which is quite tiny.

If we consider detection using only the axion-induced electric field E_a , a Fabry-Pérot (FP) cavity with finesse $\mathcal{F} = 10^4$ can boost the signal according to

$$\psi_a \rightarrow \left(\frac{2\mathcal{F}}{\pi}\right) \psi_a \approx 1.3 \times 10^{-10} \text{ rad}, \quad (12)$$

which would yield an $\text{SNR}_{\text{FP}} \sim 0.04$, which is insufficient for detection. However, we will see next how using a probe radio-frequency (RF) beam at the axion frequency of oscillation can further enhance the signal.

A. Probing Method with Electro-Optic Readout

The axion-induced oscillating electric field modulates the birefringence of the EO crystal, imprinting a small ellipticity or phase shift onto the laser polarization. To enhance the readout signal, we introduce an RF tone at the cavity resonance frequency, which coherently interferes with the axion-induced field inside the cavity. The probing method effectively amplifies the signal by creating a beat between the injected RF field and the axion signal, leading to a variance in the optical response that is detectable with high sensitivity. This technique, originally developed for microwave detection using power detectors [1], is applied in the EO axion signal detection here, for the first time.

Since the detection occurs via polarization rotation (ellipticity) in the optical field—not via amplification of the microwave field itself—the signal readout is not constrained by the standard quantum limit. Furthermore, because the probing method effectively decouples the signal strength from the laser power, the system can operate at low optical intensities, minimizing thermal loading on the cryogenic environment.

Operating at cryogenic temperatures ($T \lesssim 100 \text{ mK}$), the thermal photon background for a single photon detector is exponentially suppressed. However, quantum field fluctuations still exist for the method suggested here, albeit significantly reduced. Combined with the narrow bandwidth of a high- Q_c cavity, this results in a low-noise environment ideal for detecting weak axion-induced fields. The result is a highly sensitive, compact, and scalable architecture for axion detection in the 0.5–50 GHz range; in principle the lower range can be further reduced.

Next, we will examine implementing the probing method to provide a feasible detection approach, without FP enhancement. We will consider an injected RF power $P = 2 \text{ nW} = 2 \times 10^{-9} \text{ W}$. The electric field amplitude, for $\omega = 2\pi \times 10^{10} \text{ rad Hz}$, is:

$$E_{\text{probe}} = \sqrt{\frac{Q_c P}{\epsilon_0 V \omega}} \approx 0.1 \text{ V/m} \quad (13)$$

In the probing method, we are interested in detecting the fluctuations of the ellipticity, which are enhanced by the RF injected power. To see this, we note that the total electric field in the cavity is given by

$$E(t) = E_{\text{probe}} \cos(\omega t) + E_a \cos(\omega t + \phi(t)), \quad (14)$$

where $\phi(t)$ is the time-dependent relative phase between the two fields.

The axion field is not perfectly monochromatic; it has a finite spectral width $\Delta\nu_a \sim 10^{-6}\nu$ due to the virialized velocity dispersion of dark matter in the galactic halo. At $\nu = 10 \text{ GHz}$, this corresponds to $\Delta\nu_a \sim 10 \text{ kHz}$ and a coherence time of

$$\tau_a \sim \frac{1}{\Delta\nu_a} \sim 0.1 \text{ ms}. \quad (15)$$

Over timescales shorter than τ_a , the axion field behaves like a coherent wave with a well-defined phase. Over longer timescales, this phase $\phi(t)$ drifts randomly, reflecting the stochastic nature of the axion field.

In the probing method, one is interested in measuring the variance of the ellipticity

$$\langle \psi^2 \rangle \propto \frac{1}{2} [E_{\text{probe}}^2 + E_a^2 + 2E_{\text{probe}}E_a \langle \cos(\phi(t)) \rangle], \quad (16)$$

where $\langle \cos(\phi(t)) \rangle$ vanishes over many coherence times, but the variance of the fluctuations is nonzero. To capture these fluctuations, one needs to have a sampling time scale $t_{\text{sample}} \lesssim \tau_a$. In the above expression (16), fast axion oscillations at $\omega \sim m_a$ have been averaged out, since they take place at time scales much shorter than t_{sample} . Physically, the probe tone mixes coherently with the axion-induced field to generate a beat signal at the difference frequency — typically in the 1–50 kHz range. This beat modulates the birefringence of the electro-optic crystal at a frequency far below the carrier, allowing low-frequency optical detection of an otherwise extremely weak GHz signal.

Given the above discussion, the detected ellipticity scales with the geometric mean of the axion and probe electric fields:

$$\psi_{\text{probe}} = \frac{\pi}{\lambda} n^3 r_{33} \sqrt{E_a E_{\text{probe}}} L \quad (17)$$

Substituting the above benchmark values, we find $\psi_{\text{probe}} \approx 7.7 \times 10^{-11} \text{ rad}$. As before, if we employ a FP cavity with a finesse \mathcal{F} , we can enhance the signal

$$\psi_{\text{probe}} \rightarrow \left(\frac{2\mathcal{F}}{\pi} \right) \psi_{\text{probe}}, \quad (18)$$

which for $\mathcal{F} = 10^4$ will result in $\psi_{\text{probe}} \approx 4.9 \times 10^{-7} \text{ rad}$.

Thus, the SNR for a 10 mW laser power and integrating for 3 s, is :

$$\text{SNR}_{\text{probe-FP}} \approx \frac{(2\mathcal{F}/\pi)\psi_{\text{probe}}}{\delta\psi_{\text{shot}}} \approx \frac{4.9 \times 10^{-7}}{3.5 \times 10^{-9}} \approx 140 \quad (19)$$

We see, from the above, that a combination of probing and FP enhancement allows for a detectable signal, easily overcoming the measurement limitations. In fact, given the size of the above SNR, we could envision that a lower laser beam power, in conjunction with a thinner EO crystal, would also suffice for the measurement.

Here, we would like to make the following two points. First, as mentioned earlier, due to the probing method, the required sampling time is set by the axion coherence time $\tau_a = Q_a/\nu$, which is $\sim 10 \text{ kHz}$, about 6 orders of magnitude below the axion frequency. Secondly, the RF probe affects both the axion signal and the quantum-thermal background. This suggests that we need to examine the associated effective SNR for the measurement further, which will do next.

B. RF probe effect on sensitivity

Vacuum fluctuations of the electromagnetic field, though classically absent, have measurable consequences in quantum electrodynamics. In particular, they give rise to the zero-point energy of each electromagnetic mode, with an average energy of $\hbar\omega/2$, and manifest as non-zero field quadratures even at zero temperature. Single-photon detectors are sensitive only to real (on-shell) photons through energy absorption, and hence they remain insensitive to these vacuum fluctuations. However, we would need to account for such off-shell effects, as discussed below.

(ii) *Quantum-thermal noise:* The average number of thermal photons in the cavity mode is:

$$\bar{n}_{\text{th}} = \frac{1}{e^{\hbar\omega/k_B T} - 1}, \quad (20)$$

where $k_B = 1.38 \times 10^{-23} \text{ J/K}$ is the Boltzmann constant. Each photon contributes an energy $\hbar\omega$, with $\hbar \equiv h/(2\pi)$, so the thermal energy associated with the cavity is:

$$U_{\text{th}} = \hbar\omega \left(\bar{n}_{\text{th}} + \frac{1}{2} \right) \quad (21)$$

with the half photon constant background present due to off-shell vacuum fluctuations.

This energy is equally partitioned between the electric and magnetic fields, so the electric field energy is

$$U_E = \frac{1}{2} U_{\text{th}} \quad (22)$$

The above energy can also be expressed in terms of the electric field amplitude as

$$U_E = \frac{1}{2} \epsilon_0 V E_{\text{th}}^2. \quad (23)$$

Solving for the electric field E_{th} yields

$$E_{\text{th}} = \sqrt{\frac{U_{\text{th}}}{\epsilon_0 V}} = \sqrt{\frac{(\bar{n}_{\text{th}} + 1/2)\hbar\omega}{\epsilon_0 V}} \quad (24)$$

which represents the root-mean-square electric field amplitude of the thermal plus quantum fluctuations in the cavity. This sets the quantum noise floor for field-based detection methods.

The axion-induced power is:

$$P_a = P_0 Q_{\text{red}}, \quad (25)$$

where P_0 is a reference quantity and

$$Q_{\text{red}} \equiv \frac{Q_c Q_a}{Q_c + Q_a}. \quad (26)$$

For our benchmark choices $P_0 = 10^{-27}$ W, for $Q_c = 10^4$. The stored electric field amplitude in the resonant cavity is given by Eq.(7), as derived before

$$E_a = \sqrt{\frac{P_a Q_c}{\epsilon_0 V \omega}}.$$

Assuming an axion coherence time $\tau_a = Q_a/\nu$, the signal-to-noise ratio (SNR) due to thermal noise after an integration time t is given by:

$$\text{SNR}_{\text{th}}(t) = \frac{E_a}{E_{\text{th}}} \cdot \sqrt{\frac{t}{\tau_a}}, \quad (27)$$

which yields

$$\text{SNR}_{\text{th}}(t) = \sqrt{\frac{P_0 Q_{\text{red}} Q_c t}{2\pi(\bar{n}_{\text{th}} + \frac{1}{2})\hbar\omega Q_a}}, \quad (28)$$

valid when $Q_c \leq Q_a$. A more general formula—valid across both classical and quantum limits and for arbitrary cavity quality factors—is derived in the Supplemental Material, Eq. 50

$$\boxed{\text{SNR}(t) = \sqrt{\frac{P_0 Q_{\text{red}} t}{\pi \hbar \omega \coth(\frac{\hbar\omega}{2k_B T})}}}. \quad (29)$$

This expression smoothly interpolates between the quantum regime at low temperatures (where $\coth \rightarrow 1$) and the classical limit at high temperatures (where $\coth \rightarrow \frac{2k_B T}{\hbar\omega}$).

As detailed in the Supplemental Material, the thermal noise field contributing to signal detection is not determined solely by the total thermal energy stored in the cavity mode but by the fraction of this energy that spectrally overlaps with the axion signal bandwidth. In the regime where the cavity quality factor is much smaller than the axion coherence quality factor ($Q_c \ll Q_a$), only thermal fluctuations within a bandwidth $\Delta\nu \sim \nu/Q_a$ contribute effectively to the signal readout. This leads

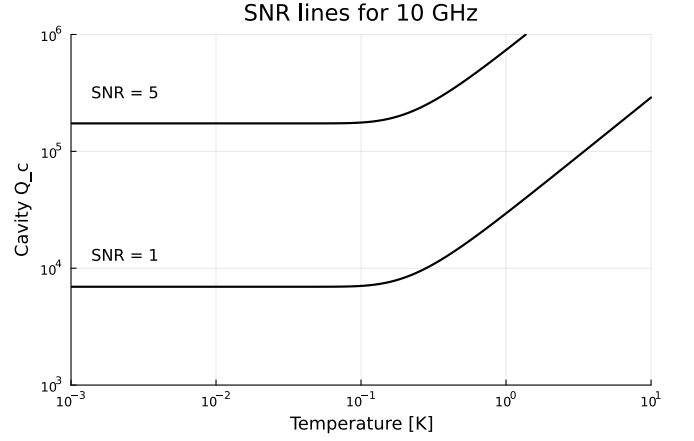


FIG. 2: Signal-to-noise ratio (SNR) as a function of Q_c and T at different operating frequencies. The transition from the quantum regime to the classical regime becomes apparent around 480 mK, where the thermal photon occupation number begins to exceed the vacuum (zero-point) contribution. The cavity volume is kept constant at 3.7 liters. The axion to photon conversion power is kept at 10^{-23} W assuming $Q_c = 10^4$, $t = 3$ s, and scaled appropriately for different cavity quality factor values; see Supplemental Material.

to a suppression of the thermal noise electric field amplitude by a factor $\sqrt{Q_c/Q_a}$, since the axion signal is narrow band while the cavity noise is broadband. The probing method, by isolating this narrow interference bandwidth, enables a higher SNR despite a broad cavity response. Figure 2 illustrates this effect for the representative case at 10 GHz, showing how SNR depends on both temperature and cavity quality factor, and highlighting the transition between quantum and classical thermal noise regimes.

The $\sqrt{Q_c/Q_a}$ thermal noise suppression can also be recovered without probing, provided that the cavity output is analyzed with frequency resolution matched to the axion linewidth $\Delta\nu_a = \nu/Q_a$. In this case, only the thermal noise within a single high-resolution Fourier transform bin contributes, and the SNR expression remains equivalent. However, the probing method achieves the same filtering effect automatically through beat-based detection.

III. DISCUSSION: SURPASSING THE LASER QUANTUM NOISE LIMIT

The combination of the probing method—where a known RF signal is injected into the system—and FP enhancement enables a substantial amplification of the signal. In particular, the induced ellipticity benefits from the geometric mean field $\sqrt{E_a E_{\text{probe}}}$, effectively boosting the axion signal strength. This hybrid approach allows the experiment to surpass the traditional quantum

shot-noise limit associated with laser light. As shown in Fig. 2 of Ref. [1], the injection of probe photons significantly enhances the signal-to-noise ratio (SNR) when the laser shot noise exceeds the sampling rate, corresponding to regions II and III in the figure. In contrast, when the shot noise is lower than the sampling rate (regions I and IV), the addition of probing power leads to reduced SNR due to unnecessary variance amplification in the electro-optic signal readout.

Owing to the resulting enhancement in signal-to-noise ratio (SNR)—by several orders of magnitude—this method offers considerable flexibility in experimental design. For example, one can reduce the laser power from 10 mW to 1 mW, while maintaining sensitivity to axions with DFSZ-level coupling. Future developments could include spatially optimized electro-optic (EO) geometries and dynamic modulation of the probe signal to further suppress noise and improve detection fidelity. Since the axion-probe beat signal appears at low frequencies (typically 1–50 kHz), laser phase noise is not a limiting factor, provided a low-noise narrow-linewidth laser is used. Locking the laser to a Fabry–Pérot cavity further suppresses phase fluctuations in this band. While probing techniques can, in principle, introduce their own quantum limits, in the present optical readout scheme such effects are not expected to pose a significant limitation. The dominant quantum noise source remains the vacuum fluctuations of the resonant cavity field. Since the injected RF probe is a coherent classical signal and the detection process involves measuring optical ellipticity rather than amplifying the microwave field, any additional quantum noise introduced by probing is expected to lie below the vacuum noise floor. As such, the overall sensitivity is ultimately limited by the cavity’s zero-point fluctuations, which are already accounted for in our analysis.

Until practical single-photon detectors become available in the GHz regime [50–57], the method presented here offers a compelling enhancement in both sensitivity and scanning speed. Specifically, this approach can accelerate axion searches by more than an order of magnitude through two mechanisms. First, by injecting a coherent probe tone and detecting the axion-induced beat signal via an EO crystal, the effective SNR exceeds the noise limit of conventional haloscopes by a factor of 5–10 [18, 20, 29, 37, 58–73]. Since the scanning rate scales inversely with the square of the SNR, this corresponds to a 25–100× increase in scanning speed while still achieving DFSZ sensitivity, even with the modest integration time of 3 seconds per frequency step assumed throughout this work. Second, the same Fabry–Pérot laser readout system can be used uniformly across a wide frequency range—from 0.5 GHz to at least 50 GHz—without reconfiguring the detection chain. This broadband capability is a critical advantage over conventional linear amplifiers and quantum-limited photon counters, which typically require frequency-specific optimization. Together, these features make the present method a versatile and pow-

erful strategy for exploring the high-frequency axion parameter space that remains largely open.

Leveraging Axion Spatial Coherence

An immediate and practical extension of the present method would be to deploy a modest array of probing haloscopes operating in parallel. Given that vacuum fluctuations are uncorrelated between separate cavities, while the axion field remains spatially coherent over macroscopic scales, coherently combining the outputs of N detectors leads to a signal that scales as N , while the noise grows only as \sqrt{N} . Thus, the overall signal-to-noise ratio improves as

$$\text{SNR}_{\text{total}} \propto \frac{N}{\sqrt{N}} = \sqrt{N} \quad ,$$

for fixed total integration time, equivalent to a single search with a volume NV .

This strategy is justified by the fact that the axion field is expected to behave as a classical, spatially coherent oscillation over a characteristic coherence length

$$\ell_{\text{coh}} \sim \frac{2\pi}{m_a v} \sim 100 \text{ m to } 1 \text{ km}, \quad (30)$$

depending on the axion mass m_a (or frequency ν_a) and its virial velocity $v \sim 10^{-3}c$. For example, at $\nu_a = 1$ GHz, the coherence length is approximately 200 m, ensuring that ten or more detectors within this radius observe the same axion phase and can be summed coherently.

The distinction between coherent axion signal and incoherent quantum or thermal noise is especially important when targeting higher-frequency axions. In that regime, the resonant cavity volume must shrink to maintain the desired frequency, limiting the available signal power. One can compensate for the loss of volume by launching several experiments in parallel, tuned at the same frequency. Since the optical Fabry–Pérot readout system is compact, stable, and easily replicated, a ten-fold array is straightforward to implement with current technology and could provide the required improvement in sensitivity or scanning rate—without introducing additional quantum or thermal noise limitations.

Implications for Axion Haloscopes

We note that the EO-based electric field readout method, especially when combined with probing, could offer significant advantages to other haloscope-style axion experiments, such as, e.g., ADMX, MADMAX and ALPHA.

In MADMAX, the dielectric disk configuration enhances axion-photon conversion but currently requires

extremely low noise power detection. Incorporating EO-based field readout could allow detection of the same signal with reduced thermal and quantum noise concerns, potentially allowing operation at 1 K or even higher.

The ALPHA experiment also operates at higher frequencies in compact resonators and faces similar challenges from quantum noise and dilution refrigeration complexity. Because EO readout responds to electric field amplitude rather than energy, it provides a more favorable SNR scaling and offers a path forward for simplified cryogenic operation. A key advantage of the proposed approach is the elimination of readout noise as a limiting factor in axion detection. By replacing conventional RF amplification chains with an optical probing system using a coherent laser and Fabry-Pérot interferometry, we suppress the dominant quantum and thermal noise sources that typically constrain integration times. This unlocks significantly faster scanning rates and ensures sensitivity to axion signals across a wide frequency range—independent of the electronic noise floor that currently limits haloscope performance.

Together, these implications suggest that EO-based probing methods, represent a compelling new detection paradigm for future axion searches.

IV. SUMMARY

In summary, the CARMEL approach unifies optical and RF techniques to achieve axion dark matter detection with enhanced sensitivity beyond the quantum noise limit. Its ability to operate across a broad frequency range, with low optical power and without complex quantum amplifiers, opens a scalable path forward in the high-frequency regime. The method is complementary to existing axion haloscopes and provides a versatile platform for future axion dark matter searches. The estimated reach of the method described in this work can cover much, and perhaps all [17], the relevant parameter space for post-inflationary axion dark matter, and potentially lead to a breakthrough in our understanding of puzzles in both the sub-atomic realm of hadronic interactions, and the large scale structure of the Universe.

ACKNOWLEDGMENTS

The work of H.D. is supported by the US Department of Energy under Grant Contract DE-SC0012704. YKS is indebted to KAIST and in particular to the Physics Department for support to finish this work. YKS acknowledges fruitful discussions with Junu Jeong on the impact of zero-point fluctuations on the signal-to-noise ratio in single versus multiple cavity configurations.

V. SUPPLEMENTAL MATERIAL

VI. SIGNAL-TO-NOISE RATIO DEPENDENCE ON QUALITY FACTOR AND TEMPERATURE

Here, we clarify the proper use of thermal noise field expressions and demonstrate how the probing method automatically reduces the thermal noise and improves the signal-to-noise ratio (SNR), especially when the cavity quality factor is lower than the axion coherence quality factor, $Q_c \ll Q_a$. The same effect can be achieved by effectively integrating over the axion band width.

1. Thermal Noise in a Resonant Cavity Mode

For a single resonant mode at angular frequency $\omega = 2\pi\nu$, the average thermal energy in the mode is:

$$U_{\text{mode}} = (n_{\text{th}} + \frac{1}{2}) \hbar\omega, \quad (31)$$

where $n_{\text{th}} = 1/(e^{\hbar\omega/k_B T} - 1)$ is the thermal occupation number.

This energy is shared equally between the electric and magnetic fields. The electric field RMS amplitude is therefore:

$$E_{\text{th}}^{(\text{mode})} = \sqrt{\frac{(n_{\text{th}} + \frac{1}{2}) \hbar\omega}{\epsilon_0 V}}, \quad (32)$$

where V is the effective mode volume. In a more compact form $U_{\text{mode}} = \frac{\hbar\omega}{2} \coth\left(\frac{\hbar\omega}{2k_B T}\right)$ and so,

$$E_{\text{th}}^{(\text{mode})} = \sqrt{\frac{\hbar\omega \coth\left(\frac{\hbar\omega}{2k_B T}\right)}{2\epsilon_0 V}}, \quad (33)$$

which is valid in both the classical and quantum limit.

2. Thermal Noise in a Band-Limited Measurement

In the classical limit, the thermal noise has a flat power spectral density near GHz frequencies, given by:

$$dP_{\text{noise}}/d\nu = k_B T \quad [\text{W/Hz}]. \quad (34)$$

When a detector samples a bandwidth $\Delta\nu$ for a time Δt , the total thermal energy collected is:

$$U = k_B T \cdot \Delta\nu \cdot \Delta t. \quad (35)$$

Assuming half of this energy contributes to the electric field and half to the magnetic field [49], the corresponding RMS E-field amplitude is:

$$E_{\text{th}}^{(\text{probe})} = \sqrt{\frac{k_B T \cdot \Delta\nu \cdot \Delta t}{\epsilon_0 V}}. \quad (36)$$

Let us introduce the reduced quality factor $Q_{\text{red}} = Q_a Q_c / (Q_a + Q_c)$, which we will use below.

3. The Effect of Probing on SNR in the $Q_c \ll Q_a$ Regime

In the regime $Q_c \ll Q_a$, the axion signal is spectrally narrow ($\Delta\nu_a = \omega/2\pi Q_a$), but the cavity bandwidth $\Delta\nu_c = \omega/2\pi Q_c$ is broad. This mismatch would ordinarily result in collecting excess thermal noise.

However, the probing method changes this: a narrow-band probe tone is injected at frequency ω_p near the axion frequency ω_a , and the detection system is sensitive only to the interference between the axion field and the probe. This effectively limits the measurement bandwidth to $\Delta\nu = \omega/(2\pi Q_a)$, matching the axion coherence bandwidth. Since the axion field is coherent over a time $\tau_a = Q_a/\nu$ (more accurately, $\tau_{\text{coherence}} = (Q_a + Q_c)/\nu$, but we will use the above definition for simplicity when $Q_c \ll Q_a$), the measurement remains Fourier-limited with $\Delta\nu \cdot \tau_a = 1$. The same effect is obtained by integrating the signal only over the axion band width. If this is not possible, the probing can be used to achieve the narrow filtering automatically.

Although the cavity supports thermal noise across its full bandwidth, only thermal fluctuations within the narrow axion bandwidth contribute to the detected beat signal. This acts as an effective filtering mechanism, and the resulting thermal noise field is reduced by a factor $\sqrt{Q_c/Q_a}$ compared to the full cavity thermal field:

$$E_{\text{th}}^{(\text{probe})} = \sqrt{\frac{k_B T}{\epsilon_0 V}} \cdot \sqrt{\frac{Q_c}{Q_a}}. \quad (37)$$

More generally, the reduction is equal to $\sqrt{(Q_{\text{red}}/Q_a)}$:

$$E_{\text{th}}^{(\text{probe})} = \sqrt{\frac{k_B T Q_{\text{red}}}{\epsilon_0 V Q_a}}. \quad (38)$$

The axion to photon conversion power scales as $P_a = P_0[(Q_c Q_a)/(Q_c + Q_a)] = P_0 Q_{\text{red}}$, with $P_0 = 10^{-23} \text{ W}/10^4$. The axion-induced field becomes:

$$E_a = \sqrt{\frac{P_0 Q_{\text{red}} Q_c}{\epsilon_0 V \omega}}. \quad (39)$$

The resulting SNR is:

$$\text{SNR}(t) = \frac{E_a}{E_{\text{th}}^{(\text{probe})}} \cdot \sqrt{\frac{t}{\tau_a}} = \sqrt{\frac{P_0 Q_c t}{2\pi k_B T}}. \quad (40)$$

The integrated SNR over time t is proportional to $\sqrt{Q_c t/T}$ and independent of the axion Q_a . The more general equation is given by:

$$\text{SNR}(t) = \frac{E_a}{E_{\text{th}}^{(\text{probe})}} \cdot \sqrt{\frac{t}{\tau_a}} = \sqrt{\frac{P_0 Q_{\text{red}} t}{2\pi k_B T}}. \quad (41)$$

which reduces to Eq. 40 above when the cavity quality factor $Q_c \ll Q_a$.

4. The Effect of Cavity Narrowness on SNR in the $Q_c \gg Q_a$ Regime

When $Q_c \gg Q_a$, the cavity is narrower than the axion linewidth. The axion power saturates:

$$P_a \approx P_0 Q_a, \quad (42)$$

and the axion induced electric field amplitude becomes:

$$E_a = \sqrt{\frac{P_0 Q_a Q_c}{\epsilon_0 V \omega}}, \quad (43)$$

while the thermal noise field:

$$E_{\text{th}} = \sqrt{\frac{k_B T}{\epsilon_0 V}}. \quad (44)$$

Using $\tau_{\text{coherence}} = (Q_c + Q_a)/\nu \approx Q_c/\nu$, the SNR becomes:

$$\text{SNR}(t) = \frac{E_a}{E_{\text{th}}} \cdot \sqrt{\frac{t}{\tau_{\text{coherence}}}} = \sqrt{\frac{P_0 Q_a t}{2\pi k_B T}}, \quad (45)$$

which can also result from Eq. 41 above for $Q_c \gg Q_a$. The integrated SNR is now proportional to $\sqrt{Q_a t/T}$ and independent of the cavity Q_c . The SNR scaling as $\sqrt{Q_c}$ holds only when $Q_c \lesssim Q_a$. For $Q_c \gg Q_a$, two competing effects emerge: while the cavity field amplitude continues to increase with Q_c , so does the thermal noise field, since the narrower cavity mode enhances thermal fluctuations per unit bandwidth despite admitting less total bandwidth. Simultaneously, only a fraction Q_a/Q_c of the axion power spectrally overlaps with the cavity mode. These effects combine to cancel any further SNR gain, leading to saturation as Q_c increases. The optimal regime is therefore $Q_c \approx Q_a$, where both the axion power and the thermal noise are spectrally matched. Future advances in single-photon detectors will be critical for pushing axion sensitivity further, particularly at low temperatures since they don't suffer from limitations due to zero point fluctuations [50–57].

5. General SNR Expression Including Quantum Fluctuations

For a single resonant mode at angular frequency $\omega = 2\pi\nu$, the average thermal energy in the mode is:

$$U_{\text{mode}} = (n_{\text{th}} + \frac{1}{2}) \hbar\omega, \quad (46)$$

where $n_{\text{th}} = 1/(e^{\hbar\omega/k_B T} - 1)$ is the thermal occupation number.

This energy is shared equally between the electric and magnetic fields. The electric field RMS amplitude is therefore:

$$E_{\text{th}}^{(\text{mode})} = \sqrt{\frac{(n_{\text{th}} + \frac{1}{2}) \hbar\omega}{\epsilon_0 V}}, \quad (47)$$

where V is the effective mode volume. In a more compact form $U_{\text{mode}} = \frac{\hbar\omega}{2} \coth\left(\frac{\hbar\omega}{2k_B T}\right)$ and so,

$$E_{\text{th}}^{(\text{mode})} = \sqrt{\frac{\hbar\omega \coth\left(\frac{\hbar\omega}{2k_B T}\right)}{2\epsilon_0 V}}, \quad (48)$$

which is valid in both the classical and quantum limit. Then, similarly as above, the thermal noise within the relevant band width is:

$$E_{\text{th}}^{(\text{probe})} = \sqrt{\frac{\hbar\omega \coth\left(\frac{\hbar\omega}{2k_B T}\right) Q_{\text{red}}}{2\epsilon_0 V Q_a}}, \quad (49)$$

This allows one to define the SNR in the quantum-

limited regime as:

$$\text{SNR}(t) = \frac{E_a}{E_{\text{th}}^{\text{probe}}} \cdot \sqrt{\frac{t}{\tau_{\text{coherence}}}} = \sqrt{\frac{P_0 Q_{\text{red}} t}{\pi \hbar\omega \coth\left(\frac{\hbar\omega}{2k_B T}\right)}}, \quad (50)$$

which is the most general equation valid in both the classical ($k_B T \gg \hbar\omega$) and quantum ($k_B T \ll \hbar\omega$) regimes and all values of the cavity quality factors. For completeness, in the quantum limit, the SNR becomes:

$$\text{SNR}(t) = \frac{E_a}{E_{\text{th}}} \cdot \sqrt{\frac{t}{\tau_{\text{coherence}}}} = \sqrt{\frac{P_0 Q_{\text{red}} t}{\pi \hbar\omega}}. \quad (51)$$

Thus, by using probing to reduce thermal noise and understanding the interplay with vacuum fluctuations, one can access high-SNR regimes even when the cavity quality factor is not ideally matched to the axion coherence.

The SNR scales as $1/\sqrt{T}$ and benefits from $\sqrt{Q_c}$ up to the axion quality factor Q_a . In the quantum regime, SNR is leveled off at low temperatures and it improves with increasing $\sqrt{Q_c}$, again up to the axion quality factor. Figure 3 shows that it is possible to overcome the thermal noise background by employing a combination of low temperature and high cavity quality factor.

-
- [1] Z. Omarov, J. Jeong, and Y. K. Semertzidis, Speeding axion haloscope experiments using heterodyne-variance-based detection with a power meter, *Phys. Rev. D* **107**, 103005 (2023).
 - [2] S. Weinberg, A new light boson?, *Phys. Rev. Lett.* **40**, 223 (1978).
 - [3] F. Wilczek, Problem of strong P and T invariance in the presence of instantons, *Phys. Rev. Lett.* **40**, 229 (1978).
 - [4] R. D. Peccei and H. R. Quinn, CP Conservation in the Presence of Instantons, *Phys. Rev. Lett.* **38**, 1440 (1977).
 - [5] R. D. Peccei and H. R. Quinn, Constraints Imposed by CP Conservation in the Presence of Instantons, *Phys. Rev. D* **16**, 1791 (1977).
 - [6] J. Preskill, M. B. Wise, and F. Wilczek, Cosmology of the Invisible Axion, *Phys. Lett. B* **120**, 127 (1983).
 - [7] P. Sikivie, Experimental tests of the “invisible” axion, *Phys. Rev. Lett.* **51**, 1415 (1983).
 - [8] M. Dine, W. Fischler, and M. Srednicki, A Simple Solution to the Strong CP Problem with a Harmless Axion, *Phys. Lett. B* **104**, 199 (1981).
 - [9] D. E. Kaplan, T. Melia, and S. Rajendran, What can solve the strong cp problem? (2025), arXiv:2505.08358 [hep-ph].
 - [10] D. J. E. Marsh, Axion Cosmology, *Phys. Rept.* **643**, 1 (2016), arXiv:1510.07633 [astro-ph.CO].
 - [11] E. Berkowitz, M. I. Buchoff, and E. Rinaldi, Lattice QCD input for axion cosmology, *Phys. Rev. D* **92**, 034507 (2015), arXiv:1505.07455 [hep-ph].
 - [12] G. Ballesteros, J. Redondo, A. Ringwald, and C. Tamarit, Unifying inflation with the axion, dark matter, baryogenesis and the seesaw mechanism, *Phys. Rev. Lett.* **118**, 071802 (2017), arXiv:1608.05414 [hep-ph].
 - [13] S. Borsanyi *et al.*, Calculation of the axion mass based on high-temperature lattice quantum chromodynamics, *Nature* **539**, 69 (2016), arXiv:1606.07494 [hep-lat].
 - [14] M. Dine, P. Draper, L. Stephenson-Haskins, and D. Xu, Axions, Instantons, and the Lattice, *Phys. Rev. D* **96**, 095001 (2017), arXiv:1705.00676 [hep-ph].
 - [15] V. B. Klaer and G. D. Moore, The dark-matter axion mass, *JCAP* **11**, 049, arXiv:1708.07521 [hep-ph].
 - [16] M. Buschmann, J. W. Foster, and B. R. Safdi, Early-Universe Simulations of the Cosmological Axion, *Phys. Rev. Lett.* **124**, 161103 (2020), arXiv:1906.00967 [astro-ph.CO].
 - [17] M. Buschmann, J. W. Foster, A. Hook, A. Peterson, D. E. Willcox, W. Zhang, and B. R. Safdi, Dark matter from axion strings with adaptive mesh refinement, *Nature Commun.* **13**, 1049 (2022), arXiv:2108.05368 [hep-ph].
 - [18] N. Du *et al.* (ADMX), Search for invisible axion dark matter with the axion dark matter experiment, *Phys. Rev. Lett.* **120**, 151301 (2018).
 - [19] C. Bartram *et al.* (ADMX Collaboration), Axion dark matter experiment: Run 1B analysis details, *Phys. Rev. D* **103**, 032002 (2021).
 - [20] C. Bartram *et al.* (ADMX), Search for invisible axion dark matter in the 3.3 – 4.2 μeV mass range, *Phys. Rev. Lett.* **127**, 261803 (2021).
 - [21] C. Boutan, B. H. LaRoque, E. Lentz, N. S. Oblath, M. S. Taubman, J. Tedeschi, J. Yang, A. M. Jones, T. Braine, N. Crisosto, L. J. Rosenberg, G. Rybka, D. Will, D. Zhang, S. Kimes, R. Ottens, C. Bartram, D. Bowring, R. Cervantes, A. S. Chou, S. Knirck, D. V. Mitchell, A. Sonnenschein, W. Wester, R. Khatiwada,

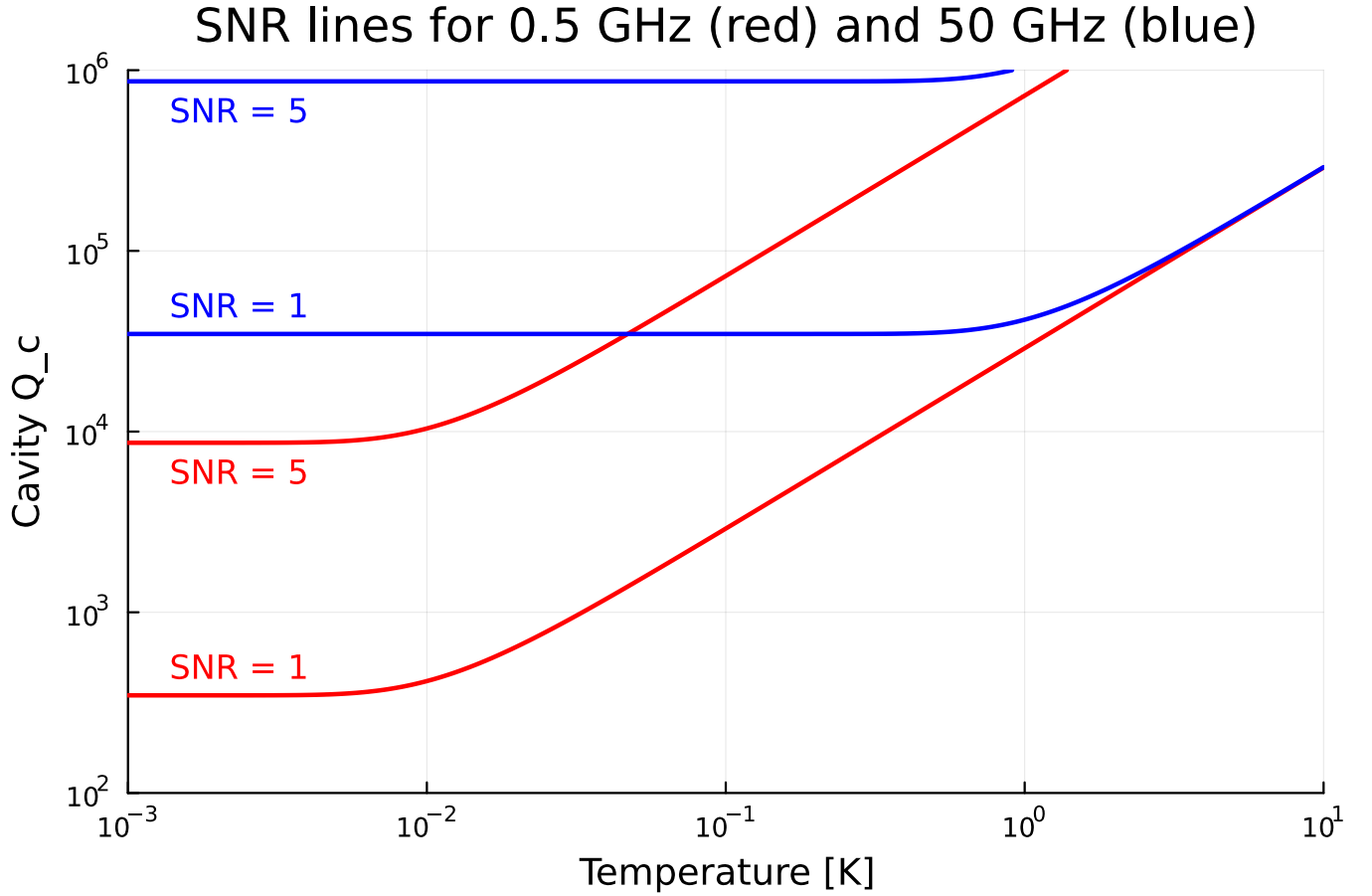


FIG. 3: Signal-to-noise ratio (SNR) as a function of Q_c and T at different operating frequencies. The transition from the quantum regime to the classical regime becomes apparent around 24 mK for 0.5 GHz (red), and 2.4 K for 50 GHz (blue), where the thermal photon occupation number begins to exceed the vacuum (zero-point) contribution. The cavity volume is kept constant at 3.7 liters. The axion to photon conversion power is kept at 10^{-23} W assuming $Q_c = 10^4$ and scaled appropriately for different cavity quality factor values; see text.

- G. Carosi, N. Du, S. Durham, S. R. O'Kelley, N. Woollett, L. D. Duffy, R. Bradley, J. Clarke, I. Siddiqi, A. Agrawal, A. V. Dixit, J. R. Gleason, A. T. Hipp, S. Jois, P. Sikivie, N. S. Sullivan, D. B. Tanner, J. H. Buckley, C. Gaikwad, E. A. Henriksen, J. Hoffman, K. W. Murch, P. M. Harrington, E. J. Daw, M. G. Perry, and G. C. Hilton (ADMX Collaboration), Axion dark matter experiment: Run 1a analysis details, *Phys. Rev. D* **109**, 012009 (2024).
- [22] C. Goodman, M. Guzzetti, C. Hanretty, L. J. Rosenberg, G. Rybka, J. Sinnis, D. Zhang, J. Clarke, I. Siddiqi, A. S. Chou, M. Hollister, S. Knirck, A. Sonnenschein, T. J. Caligiure, J. R. Gleason, A. T. Hipp, P. Sikivie, M. E. Solano, N. S. Sullivan, D. B. Tanner, R. Khatriwada, G. Carosi, C. Cisneros, N. Du, N. Robertson, N. Woollett, L. D. Duffy, C. Boutan, T. Braine, E. Lentz, N. S. Oblath, M. S. Taubman, E. J. Daw, C. Mostyn, M. G. Perry, C. Bartram, T. A. Dyson, S. Ruppert, M. O. Withers, C. L. Kuo, B. T. McAllister, J. H. Buckley, C. Gaikwad, J. Hoffman, K. Murch, M. Goryachev, E. Hartman, A. Quiskamp, and M. E. Tobar (ADMX Collaboration), Admx axion dark matter bounds around 3.3 μeV with dine-fischler-srednicki-zhitnitsky discovery ability, *Phys. Rev. Lett.* **134**, 111002 (2025).
- [23] C. J. O'Hare, Axionlimits: Data and plots for axion-photon coupling limits, <https://github.com/cajohare/AxionLimits> (2020).
- [24] J. E. Kim, Weak Interaction Singlet and Strong CP Invariance, *Phys. Rev. Lett.* **43**, 103 (1979).
- [25] M. A. Shifman, A. I. Vainshtein, and V. I. Zakharov, Can Confinement Ensure Natural CP Invariance of Strong Interactions?, *Nucl. Phys. B* **166**, 493 (1980).
- [26] A. R. Zhitnitsky, On Possible Suppression of the Axion Hadron Interactions. (In Russian), *Sov. J. Nucl. Phys.* **31**, 260 (1980).
- [27] J. Jeong, S. Youn, S. Ahn, J. E. Kim, and Y. K. Semertzidis, Concept of multiple-cell cavity for axion dark matter search, *Physics Letters B* **777**, 412 (2018).
- [28] S. Bae, S. Youn, and J. Jeong, Tunable photonic crystal haloscope for high-mass axion searches, *Phys. Rev. D* **107**, 015012 (2023).
- [29] S. Bae, J. Jeong, Y. Kim, S. Youn, H. Park, T. Seong, S. Oh, and Y. K. Semertzidis, Search for dark matter axions with tunable tm_{020} mode, *Phys. Rev. Lett.* **133**, 211803 (2024).
- [30] J. Kim *et al.*, Exploiting higher-order resonant modes for

- axion haloscopes, *J. Phys. G* **47**, 035203 (2020).
- [31] J. Jeong, S. Youn, and Y. K. Semertzidis, Horn-array haloscope for volume-efficient broadband axion searches, *Phys. Rev. D* **108**, L051101 (2023).
 - [32] A. Caldwell *et al.*, Dielectric haloscopes: A new way to detect axion dark matter, *Phys. Rev. Lett.* **118**, 091801 (2017).
 - [33] P. Brun, A. Caldwell, L. Chevalier, G. Dvali, P. Freire, E. Garutti, S. Heyminck, J. Jochum, S. Knirck, M. Kramer, C. Krieger, T. Lasserre, C. Lee, X. Li, A. Lindner, B. Majorovits, S. Martens, M. Matysek, A. Millar, G. Raffelt, J. Redondo, O. Reimann, A. Ringwald, K. Saikawa, J. Schaffran, A. Schmidt, J. Schütte-Engel, F. Steffen, C. Strandhagen, G. Wieching, and MADMAX Collaboration, A new experimental approach to probe QCD axion dark matter in the mass range above 40 eV, *The European Physical Journal C* **79**, 186 (2019).
 - [34] T. M. collaboration, S. Knirck, J. Schütte-Engel, S. Beurthey, D. Breitmoser, A. Caldwell, C. Diaconu, J. Diehl, J. Egge, M. Esposito, A. Gardikiotis, E. Garutti, S. Heyminck, F. Hubaut, J. Jochum, P. Karst, M. Kramer, C. Krieger, D. Labat, C. Lee, X. Li, A. Lindner, B. Majorovits, S. Martens, M. Matysek, E. Öz, L. Planat, P. Pralavorio, G. Raffelt, A. Ranadive, J. Redondo, O. Reimann, A. Ringwald, N. Roch, J. Schaffran, A. Schmidt, L. Shtembari, F. Steffen, C. Strandhagen, D. Strom, I. Usherov, and G. Wieching, Simulating MADMAX in 3d: requirements for dielectric axion haloscopes, *Journal of Cosmology and Astroparticle Physics* **2021** (10), 034.
 - [35] J. De Miguel, A. Kryemadhi, and K. Zioutas (On behalf of the DALI Collaboration), Dali sensitivity to streaming axion dark matter, *Phys. Rev. D* **111**, 023016 (2025).
 - [36] A. J. Millar, S. M. Anlage, R. Balafendiev, P. Belov, K. van Bibber, J. Conrad, M. Demarteau, A. Droster, K. Dunne, A. G. Rosso, J. E. Gudmundsson, H. Jackson, G. Kaur, T. Klaesson, N. Kowitt, M. Lawson, A. Leder, A. Miyazaki, S. Morampudi, H. V. Peiris, H. S. Røising, G. Singh, D. Sun, J. H. Thomas, F. Wilczek, S. Withington, M. Wooten, J. Dilling, M. Febbraro, S. Knirck, and C. Marvinney (Endorsers), Searching for dark matter with plasma haloscopes, *Phys. Rev. D* **107**, 055013 (2023).
 - [37] C. Adair *et al.* (CAST-CAPP), Search for dark matter axions with CAST-CAPP, *Nature Communications* **13**, 6180 (2022).
 - [38] D. Ahn *et al.*, High quality factor high-temperature superconducting microwave cavity development for the dark matter axion search in a strong magnetic field, *ArXiv 10.48550/arXiv.1902.04551* (2019), 1902.04551.
 - [39] D. Ahn, O. Kwon, W. Chung, W. Jang, D. Lee, J. Lee, S. W. Youn, D. Youm, and Y. K. Semertzidis, Maintaining high Q-factor of superconducting $\text{YBa}_2\text{Cu}_3\text{O}_{7-x}$ microwave cavity in a high magnetic field (2019), *arXiv:1904.05111 [physics.ins-det]*.
 - [40] D. Ahn, O. Kwon, W. Chung, *et al.*, Biaxially textured $\text{YBa}_2\text{Cu}_3\text{O}_{7-x}$ microwave cavity in a high magnetic field for a dark-matter axion search, *Phys. Rev. Appl.* **17**, L061005 (2022).
 - [41] R. Ebadi, D. E. Kaplan, S. Rajendran, and R. L. Walsworth, GALILEO: Galactic Axion Laser Interferometer Leveraging Electro-Optics, *Phys. Rev. Lett.* **132**, 101001 (2024), *arXiv:2306.02168 [hep-ph]*.
 - [42] C. Riek, D. V. Seletskiy, A. S. Moskalenko, J. F. Schmidt, P. Krauspe, S. Eckart, S. Eggert, G. Burkard, and A. Leitenstorfer, Direct sampling of electric-field vacuum fluctuations, *Science* **350**, 420 (2015), <https://www.science.org/doi/pdf/10.1126/science.aac9788>.
 - [43] C. Riek, P. Sulzer, M. Seeger, A. S. Moskalenko, G. Burkard, D. V. Seletskiy, and A. Leitenstorfer, Sub-cycle quantum electrodynamics, *Nature* **541**, 376 (2017).
 - [44] P. Sikivie, Clean energy from dark matter? (2021), *arXiv:2107.14300 [hep-ph]*.
 - [45] A. Yariv and P. Yeh, *Photonics: Optical Electronics in Modern Communications*, 6th ed. (Oxford University Press, 2006).
 - [46] B. E. A. Saleh and M. C. Teich, *Fundamentals of Photonics*, 2nd ed. (Wiley-Interscience, 2007).
 - [47] S. Ahn, J. Kim, B. I. Ivanov, O. Kwon, H. Byun, A. F. van Loo, S. Park, J. Jeong, S. Lee, J. Kim, i. m. c. b. u. Kutlu, A. K. Yi, Y. Nakamura, S. Oh, D. Ahn, S. Bae, H. Choi, J. Choi, Y. Chong, W. Chung, V. Gkika, J. E. Kim, Y. Kim, B. R. Ko, L. Miceli, D. Lee, J. Lee, K. W. Lee, M. Lee, A. Matlashov, P. Parashar, T. Seong, Y. C. Shin, S. V. Uchaikin, S. Youn, and Y. K. Semertzidis, Extensive Search for Axion Dark Matter over 1 GHz with CAPP'S Main Axion Experiment, *Phys. Rev. X* **14**, 031023 (2024).
 - [48] D. Kim, J. Jeong, S. Youn, Y. Kim, and Y. K. Semertzidis, Revisiting the detection rate for axion haloscopes, *Journal of Cosmology and Astroparticle Physics* **2020** (03), 066.
 - [49] Y. Kim, D. Kim, J. Jeong, J. Kim, Y. C. Shin, and Y. K. Semertzidis, Effective approximation of electromagnetism for axion haloscope searches, *Physics of the Dark Universe* **26**, 100362 (2019).
 - [50] S. K. Lamoreaux, K. A. van Bibber, K. W. Lehnert, and G. Carosi, Analysis of single-photon and linear amplifier detectors for microwave cavity dark matter axion searches, *Phys. Rev. D* **88**, 035020 (2013).
 - [51] G. Oelsner, C. K. Andersen, M. Reháč, M. Schmelz, S. Anders, M. Grajcar, U. Hübner, K. Mølmer, and E. Il'ichev, Detection of weak microwave fields with an underdamped Josephson junction, *Phys. Rev. Appl.* **7**, 014012 (2017).
 - [52] L. S. Revin, A. L. Pankratov, A. V. Gordeeva, A. A. Yablokov, I. V. Rakut, V. O. Zbrozhek, and L. S. Kuzmin, Microwave photon detection by an al Josephson junction, *Beilstein Journal of Nanotechnology* **11**, 960 (2020).
 - [53] A. D'Elia, A. Rettaroli, S. Tocci, D. Babusci, C. Barone, M. Beretta, B. Buonomo, F. Chiarello, N. Chikhi, D. Di Gioacchino, G. Felici, G. Filatella, M. Fistul, L. Foggetta, C. Gatti, E. Il'ichev, C. Ligi, M. Lisitskiy, G. Maccarrone, F. Mattioli, G. Oelsner, S. Pagano, L. Piersanti, B. Ruggiero, G. Torrioli, and A. Zagoskin, Stepping closer to pulsed single microwave photon detectors for axions search, *IEEE Transactions on Applied Superconductivity* **33**, 1 (2023).
 - [54] J. Govenius, R. E. Lake, K. Y. Tan, and M. Möttönen, Detection of zeptojoule microwave pulses using electrothermal feedback in proximity-induced Josephson junctions, *Phys. Rev. Lett.* **117**, 030802 (2016).
 - [55] S. Matsuki, I. Ogawa, S. Nakamura, M. Tada, K. Yamamoto, and A. Msaiki, Rydberg-atom cavity detector for dark matter axion search in Kyoto, *Nuclear Physics B - Proceedings Supplements* **51**, 213 (1996), proceedings of the International Symposium on Sources and Detection

of Dark Matter in the Universe.

- [56] K. Kim and J. Ahn, Quantum tomography of rydberg atom graphs by configurable ancillas, *PRX Quantum* **4**, 020316 (2023).
- [57] A. L. Pankratov *et al.*, Search for dark-matter axions beyond the quantum limit: the cosmological axion sarov haloscope (cash) proposal (2025), arXiv:2506.18595 [hep-ph].
- [58] S. DePanfilis, A. C. Melissinos, B. E. Moskowitz, *et al.*, Limits on the abundance and coupling of cosmic axions at $4.5 < m_a < 5.0 \mu\text{eV}$, *Phys. Rev. Lett.* **59**, 839 (1987).
- [59] C. Hagmann, P. Sikivie, N. S. Sullivan, and D. B. Tanner, Results from a search for cosmic axions, *Phys. Rev. D* **42**, 1297 (1990).
- [60] V. Anastassopoulos, S. Aune, K. Barth, *et al.*, New cast limit on the axion-photon interaction, *Nature Physics* **13**, 584 (2017).
- [61] T. Braine *et al.* (ADMX), Extended search for the invisible axion with the axion dark matter experiment, *Phys. Rev. Lett.* **124**, 101303 (2020).
- [62] B. M. Brubaker *et al.*, First results from a microwave cavity axion search at $24 \mu\text{eV}$, *Phys. Rev. Lett.* **118**, 061302 (2017).
- [63] K. Backes *et al.*, A quantum enhanced search for dark matter axions, *Nature* **590**, 238 (2021).
- [64] M. J. Jewell *et al.* (HAYSTAC), New results from HAYSTAC's phase II operation with a squeezed state receiver, *Phys. Rev. D* **107**, 072007 (2023).
- [65] S. Lee, S. Ahn, J. Choi, B. R. Ko, and Y. K. Semertzidis, Axion dark matter search around $6.7 \mu\text{eV}$, *Phys. Rev. Lett.* **124**, 101802 (2020).
- [66] J. Kim *et al.*, Near-quantum-noise axion dark matter search at CAPP around $9.5 \mu\text{eV}$, *Phys. Rev. Lett.* **130**, 091602 (2023).
- [67] J. Jeong *et al.*, Search for invisible axion dark matter with a multiple-cell haloscope, *Phys. Rev. Lett.* **125**, 221302 (2020).
- [68] O. Kwon *et al.*, First results from an axion haloscope at CAPP around $10.7 \mu\text{eV}$, *Phys. Rev. Lett.* **126**, 191802 (2021).
- [69] A. K. Yi *et al.*, Axion dark matter search around $4.55 \mu\text{eV}$ with Dine-Fischler-Srednicki-Zhitnitskii sensitivity, *Phys. Rev. Lett.* **130**, 071002 (2023).
- [70] B. Yang, H. Yoon, M. Ahn, Y. Lee, and J. Yoo, Extended axion dark matter search using the CAPP18T haloscope, *Phys. Rev. Lett.* **131**, 081801 (2023).
- [71] Y. Lee, B. Yang, H. Yoon, *et al.*, Searching for invisible axion dark matter with an 18 T magnet haloscope, *Phys. Rev. Lett.* **128**, 241805 (2022).
- [72] Y. Kim, J. Jeong, S. Youn, S. Bae, K. Lee, A. F. van Loo, Y. Nakamura, S. Oh, T. Seong, S. Uchaikin, J. E. Kim, and Y. K. Semertzidis, Experimental search for invisible dark matter axions around $22 \mu\text{eV}$, *Phys. Rev. Lett.* **133**, 051802 (2024).
- [73] T. Grenet, R. Ballou, Q. Basto, *et al.*, The Grenoble axion haloscope platform (GrAHal): development plan and first results (2021), arXiv:2110.14406 [hep-ex].